Reduced Oxidation of Ferritic Stainless Steels at 850 °C in high H_2O/ H_2 by Coating with Cerium

Patrik Alnegren[a], Jan Grolig[a], Jan-Erik Svensson[a], Jan Froitzheim [a]

a) Energy and Materials, Chemistry and Chemical Engineering, Chalmers University of Technology

Kemivägen 10, 41296 Gothenburg, Sweden

*Corresponding author. Tel.: +46 31 772 2828; fax: +46 31 772 2853;
E-mail address: patrik.alnegren@chalmers.se
Kemivägen 10, 41296 Gothenburg, Sweden

1 Abstract

The use of cheaper steels as interconnects in solid oxide fuel cells (SOFC) and electrolysis cells (SOEC) can significantly lower total production costs, but the corrosion durability of these steels needs to be improved. Surface modification by the application of reactive element (RE) coatings shows great promise in reducing the oxidation rate of chromia-forming steels but reactive element coatings have mostly been studied in atmospheres of air. The fuel side of SOFCs and SOECs can reach high contents of steam, which, in turn, can lead to accelerated corrosion, compared to the air side. Here, we expose ferritic stainless steels Sanergy HT and the cheaper AISI 441, with and without a physical vapor deposited (PVD) 10 nm coating of Ce, to a simulated fuel gas of Ar-3% H_2- 40% H_2O at 850 °C. It is shown that the chromia scales of the coated samples are almost three times thinner after 4500 h, but the spinel top scales increase in thickness. A change from parabolic oxidation to sub-parabolic oxidation for the coated samples is also observed, which should lead to significantly longer service life of the Ce-coated steels.

2 Introduction

Solid oxide fuel cells operate through electrochemical action to convert chemical energy in hydrogen or hydrocarbon fuels into electricity and can be considered a disruptive technology in the field of electricity production. Their high operating temperature leads to low sensitivity to catalyst poisoning and also leads to fast electrode kinetics, which therefore give SOFCs the highest electrical efficiency of the fuel cell technologies. They can also be used in reverse mode for efficient production of hydrogen from steam and are, then, often referred to as solid oxide electrolysis cells (SOEC). A key component in SOFCs and SOECs is the interconnect, which most commonly is made of a ferritic stainless steel sheet that electrically connects individual cell elements (anode/electrolyte/cathode) and separates and distributes fuel and oxidant gases. Ferritic stainless steels rely on the formation of a dense, well-adhered Cr_2O_3 scale that protects the steel from rapid oxidation. However, the industry standard service lifetime of a SOFC stack is often 40 000 h, which puts high demands on the interconnect material.

Specialized steels have been developed for use as interconnects in SOFCs, e.g. Crofer 22 APU, Crofer 22 H, ZMG232, Sanergy HT, E-Brite, but to reduce the overall cost of a stack it is compelling to look

into the use of cheaper, more generic commercial steel grades. The performance of these kinds of steels in terms of long-term stability is usually not as good as for the specialized steels. Nevertheless, studies in the context of SOFC interconnects have shown so called reactive element coatings can be used to both reduce the oxidation rate and the buildup of electrical resistance of ferritic stainless steels [1–5]. So called reactive elements, such as Y, Zr, La, and Ce, when alloyed in small concentrations (~0.1 wt%), or added as surface coatings, are known to improve the oxidation properties of chromia formers in the following ways: i) improve oxide scale adherence, ii) decrease oxidation rate, and iii) promote chromia formation thus reducing the required Cr concentration in an alloy [6]. Atmospheres containing high contents of water vapor are known to promote the formation of rapidly growing Fe oxides in FeCr alloys [7]. SOFCs run with high fuel utilization or SOECs fed with high concentration steam can, thus, be challenging conditions for ferritic stainless steels. Reactive elements have classically been considered ineffective in these low-pO_2 environments [7], but in contradiction to previous beliefs, more recent studies have shown that reactive element coatings can reduce the oxidation rate [1,8] and promote chromia formation [9] also in H_2/H_2O atmospheres.

The use of the Fe18Cr steel AISI 441 as interconnect material would offer a major cost reduction compared to specialized SOFC steels, but its low content of Cr could lead to iron oxide formation in atmospheres with high steam concentration. Ardigo et al. have exposed AISI 441 to 1% H_2- 9% H_2O at 800 °C and found that an Fe-rich oxide was formed, but a protective chromia layer was also formed underneath [10]. This could indicate that this environment is close to the limiting conditions for this steel grade. In the current study, we expose AISI 441 steel to a potentially harsher environment of Ar-3% H_2-40% H_2O at 850 °C. Sanergy HT is also included as test material to act as a state-of-the-art reference. In addition, a 10 nm layer of Ce is applied to the samples with a PVD process. The purpose is to investigate if Ce-coated AISI 441 could be a commercially viable option for the fuel side of SOFC and SOEC. It is found that AISI 441 could be suitable for application as the interconnect if coated with Ce. Ce is found to both decrease the overall oxidation rate as well as to change the oxidation mechanism.

3 Experimental

The composition, as specified by the manufacturers for the specific batches, of the two studied ferritic stainless steels, Sanergy HT and AISI 441, can be found in Table 1. A 10 nm Ce layer was applied to both sides of steel sheets using a proprietary physical vapor deposition process at Sandvik Materials Technology. Samples were cut into coupons of 15 mm x 15 mm size, which were degreased with acetone and ethanol in an ultrasonic bath.

Table 1. Composition of the tested materials in wt%, as supplied by Sandvik Materials Technology.

Thickness (mm)	Fe	Cr	Mn	Si	Al	Ti	W/Mo	Nb	Zr
		17.83	0.26	0.55		0.14		0.48	
0.2	Bal	21.2	0.30	0.12	0.02	0.09	0.96Mo	0.71	0.06

Testing of the materials was done by placing the samples in simulated interconnect fuel side conditions inside a horizontal tubular furnace (Al_2O_3 tube) with an inner diameter of 46 mm. Prior to heating, the reaction chamber was flushed with dry Ar-5 % H_2. The heating rate from room temperature to 850 °C was 15 °C min^{-1}. Once the temperature was above 500 °C, the gas mixture of Ar - 5 % H_2 was bubbled through a humidifier set to 80 °C and equilibrated by a coil condenser set at a temperature of 76.4 °C, which resulted in a gas composition of Ar - 40 % H_2O - 3 % H_2. The experiment was finished by allowing natural cooling of the furnace, which was significantly slower than the heating rate. At 500 °C, the gas flow was changed to dry Ar - 5 % H_2, and the samples were removed from the furnace the following day

at near-room temperature. The total gas flow rate was 250 smL min^{-1}, which corresponds to a mean flow velocity of 1.0 cm s^{-1} inside the reaction chamber. The gas tube that connects the condenser and reaction chamber was heated above 100 °C with a heating cord to ensure that no condensation occurred. An Optidew Vision Precision Dew-Point Hygrometer (chilled mirror) was used to validate the correct water content.

The samples were exposed in both continuous and discontinuous fashion. Discontinuous exposures were performed by placing the samples back into the furnace after gravimetric analysis, which means these samples were thermally cycled. This was done to better follow the oxidation kinetics of individual samples. Continuous exposures, meaning the samples were only exposed once for a certain amount of time, were carried out to obtain samples for ex-situ analysis and to compare with the oxidation kinetics of the thermally cycled samples. Exposures were continued up to 4500 h. Plan view and cross section images of the samples, as well as compositional information, were obtained using scanning electron microscopy with a FEI Quanta FEG 200 ESEM and a Zeiss LEO ULTRA 55 FEG-SEM, both equipped with an INCA X-Sight energy-dispersive X-ray spectroscopy (EDX) system. Cross sections of samples were prepared by polishing epoxy mounted samples and by broad ion beam milling (BIB) with a Leica EM TIC 3X instrument. Grazing incidence X-ray diffraction was performed on the oxide scales of the exposed samples with a Siemens D5000 diffractometer.

4 Results

Samples of the ferritic stainless steels Sanergy HT and AISI 441 were exposed to a simulated fuel side gas of an SOC with a composition of Ar - 40 % H_2O - 3 % H_2 at 850 °C. Both as-received, uncoated samples, and samples coated with 10 nm Ce were tested up to 4500 h, and their oxidation kinetics was monitored with gravimetry and their microstructure was monitored using SEM/EDX and XRD. The increased mass of a metal can be used as a measure of the amount of oxidation and can be considered proportional to the oxide thickness if the oxide scale is dense and does not spall off during the experiment. Figure 1 shows the mass gain data from all experiments plotted against time. The mass gain of samples that were exposed only once (continuous exposures) are marked with hollow data markers, and samples that were exposed several times (discontinuous exposures) are marked with filled data markers. From this graph, it can be concluded that:

- - AISI 441 oxidizes rapidly in the initial part of the exposure.
  - Ce-coated Sanergy HT samples show slightly slower oxidation kinetics than uncoated samples.
  - Ce-coated AISI 441 oxidizes much slower than uncoated.

The oxidation kinetics and oxide morphology will be compared between the uncoated steels and the Ce-coated steels and presented in more detail in the sections below.

4.1 Uncoated steels

Figure 2 shows oxidation kinetics from a discontinuous exposure of uncoated steels, with mass gains plotted versus time on the left-hand side and squared mass gain on the right-hand side. From these graphs, it can be seen that both steels follow parabolic kinetics according to the formula:

$$\left(\frac{\Delta m}{A}\right)^2 = k_p t + C \quad (1)$$

where Δm is the change in mass, A is the total sample area, t is the exposure time, k_p is the parabolic oxidation rate constant, and C is the integration constant. This indicates that diffusion through the oxide scale is rate limiting for oxidation [11]. However, the fitted linear equation of the squared mass gain of AISI 441 does not start at zero. This would indicate that the initial oxidation is rapid, but that a change of the oxidation mechanism occurs after some time. Figure 3 shows plan view micrographs of AISI 441

after different times of exposure. In the figure, two types of oxide regions are noted for the 1- 168 h samples: a finer grained part with a less dense structure and a part with denser oxide. The elemental maps of the 168-h sample show that the different regions are either Cr-rich or Fe-rich. After 4500 h, the whole surface is covered with the finer grained porous type oxide. Figure 4 shows cross sections of the oxides formed on AISI 441, and Figure 5 shows X-ray diffractograms with identified crystal phases. The spinel peaks of AISI 441 clearly shift towards higher 2theta angles, compared to those of Sanergy HT, which would indicate that AISI 441 has formed a spinel that is more iron rich. This is in good agreement with the cross section that shows that the outer spinel phase consists of Fe, Cr, and Mn. It can be concluded from Figures 4 and 5 that the thicker oxide regions consist of a spinel phase of the type $(Fe,Cr)_3O_4$. From the 1 h-micrograph in Figure 4, it can be seen that, at some locations, a 3 µm thick oxide has formed, which means that the oxidation must be very rapid in the beginning. After 500 h, a corundum phase (Cr_2O_3) has formed underneath the Fe-rich spinel, which explains the transition to slower oxidation. This type of oxidation behavior, with an inner Cr_2O_3 and an outer $(Fe,Cr)_3O_4$, was also observed by Ardigo et. al, [10] who exposed AISI 441 to Ar- 1 % H_2- 9 % H_2O. Using gold markers and isotope tracer experiments those authors concluded that the chromia grew by inwards diffusion of oxygen, or hydroxides, and the spinel grew by cation outward diffusion. However, after 4500 h in the present study, the spinel type oxide did not seem to have grown significantly. Thus, it seems that most of the $(Fe,Cr)_3O_4$ is formed within the first hours of exposure. The chromia layer had grown to 5 µm after 4500 h and was measured with EDX to be very pure; it had cationic concentrations of Fe and Mn below 1 %. An enrichment of Mn in the lower parts of the spinel phase after 4500 h indicates outward diffusion of this element. This is expected when Mn is present in an alloy due to its relatively fast diffusion coefficient in chromia [12]. A silicon oxide layer had formed after 4500 h underneath the chromia. Due to the high electric resistance of silica, such layer could cause overall increased electrical resistance over the interconnect in an SOFC or SOEC.

The Sanergy HT samples showed protective oxidation behavior from the beginning of the exposure, i.e. the parabolic linear equation goes through the origin in the graph in Figure 2. Figure 6 shows plan view micrographs of Sanergy HT samples where it can be seen that the oxide is uniform over the surface of the samples. A larger crystallite, with a length of approximately 20 µm, is visible in the 4500-h micrograph. This type of oxide was found on several of the samples (not specifically on Sanergy HT) and was identified as Mn_2SiO_4, which probably originated from the evaporation of silica in the furnace tube due to the high water content in the experiments. Figure 7 shows micrographs of cross sections of Sanergy HT. From this figure, together with the X-ray diffractogram in Figure 5, it is possible to conclude that the oxide consists of inner Cr_2O_3 and outer $(Mn,Cr)_3O_4$, which is in agreement with observations of other authors of Mn-containing steels in both air and H_2/H_2O atmospheres [13]. After 4500 h, the $(Mn,Cr)_3O_4$ layer had a thickness of 0.6 µm, and the Cr_2O_3 layer had a thickness of 5 µm, with a Mn and Fe content lower than 1 cation%. The Si oxide on the Sanergy HT sample was enriched at the oxide/metal interface after 4500 h, but it was not as thick as the silica layer of the AISI 441 sample (Figure 4). The fact that less Si enrichment was found on Sanergy HT is likely due to the lower Si content in the alloy along with a higher Nb content, which is known to tie up Si by incorporation into Laves phase precipitates [14].

4.2 Ce-coated steels

Figure 8 shows oxidation kinetics from a discontinuous exposure of Ce-coated steels, with mass gains plotted versus time. The oxidation of Ce-coated AISI 441 was initially faster than for Ce-coated Sanergy HT, but after 4500 h, the AISI 441sample had the lowest mass gain. The initial rapid oxidation can be explained by the formation of $(Fe,Cr)_3O_4$ in the early stages of oxidation, which will be discussed more in detail below. Equation (1) can be rewritten as:

$$\frac{\Delta m}{A} = k_{\mathrm{p}}' t^{0.5} + C' \quad (2)$$

Corresponding equations were fitted to the mass gain data in Figure 8. It can be seen in the figure that Sanergy HT had a kinetics close to parabolic, i.e. an exponent close to 0.5. The oxidation of AISI 441 steel had significant sub-parabolic kinetics and an exponent of its fitted mass gain function of closer to 0.2. The amount of iron-rich spinel oxide formed on AISI 441 in the early stages of oxidation seems to have been mitigated by the Ce coating. Figure 9 shows the mass gain data of Ce-coated steels that were only exposed once plotted against time. A large variation in mass gain between the different exposures for AISI 441 the first 24 h can be seen in the figure, whereas the variation for Sanergy HT is small. Analysis of the oxide with SEM/EDX revealed that the oxide formed on the low mass gain 24-h samples, denoted A in Figure 9, was richer in Cr and Mn and that the higher mass gain AISI 441 samples, denoted B, indeed contained more Fe. Figure 10 shows plan view micrographs of AISI 441 after different times of exposure. The samples denoted A and B in Figure 9 are also shown. It can be seen that the low mass gain sample (A) has a whisker-type oxide and that the high mass gain sample (B) has a larger grained oxide, a thicker oxide, mixed with whisker-type oxide, which indicates competing reactions for $(Fe,Cr)_3O_4$ and Cr_2O_3. Significant amounts of silicates were found on the 168-h sample, and there was a general trend of more silicate crystallites on the Ce-coated samples in general. This could mean that Ce is present on the surface of the samples and catalyzes the condensation gaseous $Si(OH)_4$. Small particles of Ce oxide were found on the surface of the 4500-h sample, which means that Ce migrates outwards over time of exposure.

Figure 11 shows cross section micrographs of Ce-coated AISI 441 exposed for 168 h and 4500 h, and Figure 12 shows X-ray diffractograms after 4500 h. It can be concluded from these figures that the outer spinel phase and the inner corundum phase (Cr_2O_3) oxides have formed. The 168-h sample in Figure 11 has an outer oxide layer of $(Mn,Cr)_3O_4$, an absence of Fe, and its corresponding mass gain is similar to that of Ce-coated Sanergy HT. The 4500-h sample had higher initial mass gain and the elemental maps show the outer spinel to consist of two phases: one inner phase rich in Mn and one outer phase rich in Fe. Thus, it seems that $(Fe,Cr)_3O_4$ was formed initially, but after the formation of a chromia layer, after some time, the outward diffusion of Fe was limited and the major outward diffusion species was Mn ions. The chromia thickness after 4500 h was around 1.7 µm, and the spinel layer thickness was around 2.5 µm. An Fe content of 14 cation% was measured in the chromia, but it should be noted that since the chromia layer was thin, some Fe signal from the spinel layer and the steel should be expected. After 4500 h, significant enrichment of Si oxide was observed in the metal/oxide interface. Figure 13 shows plan view micrographs of Ce-coated Sanergy HT exposed for different times. The variation in mass gain was low for Sanergy HT, and the oxide morphology did not differ between samples. A significant amount of silicates was found on the 24-h and 500-h samples. Whisker-type oxide was found on all the samples in Figure 13. Figure 14 shows micrographs of cross sections of Ce-coated Sanergy HT exposed for 500 h and 4500 h. These samples formed outer $(Mn,Cr)_3O_4$ and inner Cr_2O_3. The elemental SIMS profile of the 500-h sample also reveals that Ce had accumulated at the chromia/spinel interface. The thickness of the oxides after 4500 h was approximately 1.3 µm $(Mn,Cr)_3O_4$ and 1.9 µm Cr_2O_3. These thicknesses do not match the mass gain of 0.83 mg cm^{-2}, which would result in a total thickness of 5.1 µm, assuming that a dense chromia had been formed. This discrepancy can likely be explained by the wrinkled surface morphology of the Ce-coated Sanergy HT sample, which results in a larger surface area. The Fe content in the chromia layer was measured to 3 cation%. An additional observation of these samples was the presence of rather large pores, with a size of up to 400 nm, at the $Cr_2O_3/(Mn,Cr)_3O_4$ interface. Some enrichment of Si oxide at the metal/oxide interface was also observed after 4500 h.

5 Discussion

5.1 Oxidation kinetics

Comparing AISI 441 and Sanergy HT steels in their uncoated state, it was found that their oxidation rate was similar after the initial rapid oxidation of AISI 441. The early oxidation of AISI 441 was found to transition from the growth of $(Fe,Cr)_3O_4$ to Cr_2O_3, which explains the reduction of oxidation rate after some time. Sanergy HT formed protective chromia from the beginning and continued oxidation was likely limited by ionic diffusion through this oxide layer throughout the exposure period, which was represented by the parabolic kinetics. The fact that a chromia layer seem to have been established very early on Sanergy HT, compared to AISI 441, can be attributed to its higher Cr content, and/or the presence of alloyed Zr, which can promote chromia formation through the reactive element effect [6]. In addition to promoting chromia formation, reactive elements are commonly reported, at least in air atmosphere, to reduce the oxidation rate constant by approximately an order of magnitude [6]. In the present study, since the rate constant of Sanergy HT is approximately half that of AISI 441, the results imply that the alloyed Zr in Sanergy HT had little influence on the oxidation rate. It is possible that Zr could be less effective in an H_2O/H_2 atmosphere, but previous studies in oxygen atmosphere resulted in about half the k_p for Sanergy HT compared to AISI 441 [16]. A 10 nm Ce coating reduced the oxidation rate of AISI 441 dramatically, and the oxidation kinetics were observed to be clearly sub-parabolic.

The effect of the coating was less pronounced for Sanergy HT when the mass gains of uncoated and Ce-coated samples were compared, but upon further investigation, it was found that the chromia thickness of the Ce-coated steel after 4500 h was almost a third of the thickness of that of the uncoated steel. This discrepancy between the mass gain and measured oxide thickness was probably due to the wrinkled surface of the coated sample. Whether this deformation of the sample surface was a consequence of the Ce coating is beyond the scope of this paper, but the same phenomenon was not observed for the AISI 441 samples. Except for this observation, it seems that the Ce coating had similar effects on both steels and, therefore, will be treated as such in the following discussion.

5.2 Oxide morphology differences between uncoated and Ce-coated steels

5.2.1 Grain size

Alloys that only form chromia as the protective oxide are often reported to oxidize faster in atmospheres of H_2O or H_2/ H_2O than in air [7]. The cause for this is still under debate, but most researchers agree that a change in the oxide morphology of the chromia to smaller grain size and a change in growth direction from predominantly outward growth to inward growth in atmospheres of H_2/ H_2O occur. A change to smaller grain size and inward oxide growth of the chromia is also what occurs when reactive elements are added to chromia forming alloys. In atmospheres of air, chromia is known to grow outwards, and the reactive element effect is commonly explained by the blocking of outward diffusing cations. Common suggested mechanisms for this are the segregation of reactive elements to the grain boundaries, which are known to be the main transport path for oxidation [17], or poisoning of the active sites for cation vacancy annihilation at the metal/oxide interface [18]. As a consequence, reactive-element-doped scales are commonly reported to grow mainly by anionic transport. The fact that this is also the case for oxide scales, which lack reactive elements, in H_2/H_2O atmospheres could explain why reactive elements are reported to be ineffective in H_2/H_2O atmospheres. For example, Zurek et al. have exposed Ni25Cr, with and without 0.1% Y, at 1050 °C and found that the oxidation rate was lowered in air atmosphere with the addition of Y, but no large difference was observed in Ar-4% H_2- 7% H_2O. Consequently, the change to smaller grain size could be attributed to the change in oxide growth direction. Figure 15 shows micrographs of the chromia layer formed after 4500 h for uncoated and Ce AISI 441 and Sanergy HT. It is clear in this figure that the chromia grains on the Ce-coated samples are smaller than the uncoated samples. This indicates that the process of the morphology change, when reactive elements are present, is more complicated than can be explained by the oxide growth direction alone.

5.2.2 Spinel

The rate of oxidation in the current study is lower than what has been reported at the same temperature in air [19], but the opposite relation is commonly reported in literature for chromia formers. This discrepancy can likely be explained by the presence of Mn in both AISI 441 and Sanergy HT steels and the subsequent formation of a $(Mn,Cr)_3O_4$ top-layer. Niewolak et al. have studied the Fe22Cr steel Crofer 22 H, both with and without alloyed Mn, in air and in Ar-H_2-H_2O at 800 °C [20]. The findings of this study were that oxidation accelerated in air atmosphere but decelerated in Ar-H_2-H_2O atmosphere. Niewolak et al. have attributed this reduction to a blocking effect caused by the spinel layer of inward diffusing O_2^- or OH^-. This is interesting since, in the current study, along with reduced chromia growth, an increase in the thickness of the spinel layers was observed for the coated steels. One can then consider that the reduction in overall oxidation is due to the promotion of the spinel layer rather than the effect of Ce on diffusion through the chromia scale. In a study by Sattari et al. the oxide scale of Ce-coated Sanergy HT exposed to air for 3000 h at 850 °C was examined in detail with transmission electron microscopy (TEM) and electron energy loss spectroscopy (EELS), and no evidence was found for the presence of Ce within the chromia or in the chromia grain boundaries [15]. Instead, enrichment of Ce was found in the spinel grain boundaries and at the air/oxide interface. This could indicate that the reduction in oxidation rate is attributed to a change of the properties inside the spinel layer. However, such an explanation does not account for the promotion of Mn diffusion through the chromia and the subsequent increase in spinel formation as observed here. One could argue, however, that Ce affects the inward transport of anions in the spinel, effectively resulting in a thinner chromia. The thinner chromia scale on Ce-coated steels would, consequently, allow for more rapid outward diffusion of Mn. It is unclear, though, how such a mechanism could account for the smaller grain size of the chromia scales on the Ce-coated samples. Fontana et al. [8] have studied reactive element-coated ferritic stainless steels in H_2-10% H_2O and found that coatings of Y_2O_3, La_2O_3 and Nd_2O_3 all significantly reduced the oxidation rate of a Mn-free Fe30Cr alloy.

5.3 Outlook and subjects for further study

More Mn diffused through the chromia scales of the Ce-coated samples, which is in contradiction with the literature. The addition of reactive elements has been found to block the outward diffusion of Fe [21] and Ni [22] diffusion, and the reduced oxidation rate is usually explained by suppressed cationic transport. Although Mn ions are known to diffuse much faster than Cr, Fe, and Ni in chromia [12], this fact does not account for the increase in diffusion observed in the presence of Ce. This might indicate that Mn diffuses via alternative pathways, or by bulk diffusion.

The decrease in oxide thickness on the Ce-coated samples could lead to lower ASR and better fuel cell performance. However, the change in the ionic conductivity of the $(Mn,Cr)_3O_4$ layer in H_2/H_2O atmosphere, compared to air, infers that the electric properties are likely to change as well. The lower pO_2 in H_2/H_2O should favor the formation of more Mn^{2+} ions, which would occupy the A site in the spinel, resulting in a spinel richer in Cr, with a composition closer to $MnCr_2O_4$ [23]. Petric and Ling [24] have measured the electrical conductivity of different spinels and reported a five-fold decrease in the conductivity of $Mn_{1.2}Cr_{1.8}O_4$ compared to Mn_3O_4 at 800 °C in air atmosphere. The value of the Cr-rich spinel is lower in that study than what has been reported for chromia at the same temperature [25]. The benefits of a Ce coating for the electrical conductivity of an interconnect in the fuel side environment are, therefore, not obvious and should be measured on oxidized coated ferritic steels in an application relevant H_2/H_2O atmosphere.

In the current study, the Ce coating could not fully suppress the Fe oxide formation on the AISI 441 steel. In a review paper [26], Hou and Stringer discuss the difference between surface applied and alloyed reactive elements and conclude that the promotion of chromia formation was only achieved in the case of alloyed reactive elements [18]. On the other hand, here, some AISI 441 samples did not form iron-

rich oxide and overall, less iron was found in the oxides of the Ce-coated samples. This indicates that there is some degree of influence on the selective oxidation of chromium, which means that optimization of the coating could make possible the use of lower alloyed ferritic steels for use as interconnects.

The mechanism of the observed sub-parabolic oxidation of Ce-coated AISI 441 steel is well worth further study since this kind of kinetics could lead to a significant increase in the service life of chromia-forming alloys. Sub-parabolic growth of alumina formers are usually explained by oxide grain growth over time, which reduces the available grain boundaries for ionic transport [27]. It is difficult to see why the presence of Ce ions, which are thought to segregate to grain boundaries, would promote grain growth. In the present study, it was shown that smaller chromia grains formed on the Ce-coated samples. However, time-resolved information of the chromia grain structure is required in order to rule out that the grains are not initially even smaller, and indeed grow during exposure.

The current study investigated the suitability of AISI 441steel in Ar-3% H_2- 40% H_2O at 850 °C. The atmosphere was chosen to represent the harsh conditions on the fuel side of an SOFC or SOEC. In air atmosphere, AISI 441 steel has been found to be prone to cracking and spalling of the oxide, which could be mitigated with a Ce coating [28]. We, however, observed no spallation regardless of a Ce coating, which is likely due to the improved adhesion is common for chromia formers in high contents of water vapor [7]. Additionally, after initial rapid oxidation, the oxidation rate of the AISI 441 steel was found to be lower than in air, so the overall performance can be concluded to be better under the tested environment conditions than in air atmosphere. The Ce coating was effective in reducing the oxidation rate of the steel, even after 4500 h, despite the small amount applied to the samples (10 nm). Consequently, these results indicate that Ce-coated AISI 441steel is viable as interconnect material even at a temperature as high as 850 °C.

6 Acknowledgments

We gratefully acknowledge the Swedish Energy Agency for funding this research.

7 References

[1] T. Brylewski, A. Gil, A. Rakowska, S. Chevalier, A. Adamczyk, J. Dabek, et al., Improving the Physicochemical Properties of Fe–25Cr Ferritic Steel for SOFC Interconnects via Y-Implantation and Y2O3-Deposition, Oxid. Met. 80 (2013) 83–111. doi:10.1007/s11085-012-9345-z.

[2] J.G. Grolig, Coated Ferritic Stainless Steels as Interconnects in Solid Oxide Fuel Cells, (2013). http://publications.lib.chalmers.se/publication/184010-coated-ferritic-stainless-steels-as-interconnects-in-solid-oxide-fuel-cells (accessed May 29, 2015).

[3] S. Fontana, R. Amendola, S. Chevalier, P. Piccardo, G. Caboche, M. Viviani, et al., Metallic interconnects for SOFC: Characterisation of corrosion resistance and conductivity evaluation at operating temperature of differently coated alloys, J. Power Sources. 171 (2007) 652–662. doi:10.1016/j.jpowsour.2007.06.255.

[4] K. Huang, P.Y. Hou, J.B. Goodenough, Reduced area specific resistance for iron-based metallic interconnects by surface oxide coatings, Mater. Res. Bull. 36 (2001) 81–95. doi:10.1016/S0025-5408(01)00506-2.

[5] G. Cabouro, G. Caboche, S. Chevalier, P. Piccardo, Opportunity of metallic interconnects for ITSOFC: Reactivity and electrical property, J. Power Sources. 156 (2006) 39–44. doi:10.1016/j.jpowsour.2005.08.039.

[6] J. Stringer, The reactive element effect in high-temperature corrosion, Mater. Sci. Eng. A. 120–121 (1989) 129–137. doi:10.1016/0921-5093(89)90730-2.

[7] W.J. Quadakkers, J. Żurek, Oxidation in Steam and Steam/Hydrogen Environments, in: Shreir's Corros., 4th ed., Elsevier, 2010: pp. 407–456. doi:10.1016/B978-044452787-5.00022-6.

[8] S. Fontana, S. Chevalier, G. Caboche, Metallic interconnects for solid oxide fuel cell: Effect of water vapour on oxidation resistance of differently coated alloys, J. Power Sources. 193 (2009) 136–145. doi:10.1016/j.jpowsour.2008.11.041.

[9] T. Sundararajan, S. Kuroda, J. Kawakita, S. Seal, High temperature corrosion of nanoceria coated 9Cr–1Mo ferritic steel in air and steam, Surf. Coatings Technol. 201 (2006) 2124–2130. doi:10.1016/j.surfcoat.2006.02.007.

[10] M.R. Ardigo, I. Popa, S. Chevalier, S. Weber, O. Heintz, M. Vilasi, Effect of Water Vapor on the Oxidation Mechanisms of a Commercial Stainless Steel for Interconnect Application in High Temperature Water Vapor Electrolysis, Oxid. Met. 79 (2012) 495–505. doi:10.1007/s11085-012-9338-y.

[11] P. Kofstad, High Temperature Corrosion, Elsevier Applied Science Publishers Ltd., New York, 1988.

[12] R.E. Lobnig, H.P. Schmidt, K. Hennesen, H.J. Grabke, Diffusion of cations in chromia layers grown on iron-base alloys, Oxid. Met. 37 (1992) 81–93. doi:10.1007/BF00665632.

[13] W.J. Quadakkers, J. Piron-Abellan, V. Shemet, L. Singheiser, Metallic interconnectors for solid oxide fuel cells – a review, Mater. High Temp. 20 (2003) 115–127. doi:10.3184/096034003782749071.

[14] J. Froitzheim, G.H. Meier, L. Niewolak, P.J. Ennis, H. Hattendorf, L. Singheiser, et al., Development of high strength ferritic steel for interconnect application in SOFCs, J. Power Sources. 178 (2008) 163–173. doi:10.1016/j.jpowsour.2007.12.028.

[15] M. Sattari, R. Sachitanand, J. Froitzheim, J.E. Svensson, T. Jonsson, The effect of Ce on the high temperature oxidation properties of a Fe–22%Cr steel: microstructural investigation and EELS analysis, Mater. High Temp. 32 (2015) 118–122. doi:10.1179/0960340914Z.00000000084.

[16] P. Alnegren, M. Sattari, J. Froitzheim, J.E. Svensson, Degradation of ferritic stainless steels under conditions used for solid oxide fuel cells and electrolyzers at varying oxygen pressures, Corros. Sci. 110 (2016) 200–212. doi:10.1016/j.corsci.2016.04.030.

[17] D. Caplan, G.I. Sproule, Effect of oxide grain structure on the high-temperature oxidation of Cr, Oxid. Met. 9 (1975) 459–472. doi:10.1007/BF00611694.

[18] P.Y. Hou, J. Stringer, The effect of reactive element additions on the selective oxidation, growth and adhesion of chromia scales, Mater. Sci. Eng. A. 202 (1995) 1–10. doi:10.1016/0921-5093(95)09798-8.

[19] J. Froitzheim, S. Canovic, M. Nikumaa, R. Sachitanand, L.G. Johansson, J.E. Svensson, Long term study of Cr evaporation and high temperature corrosion behaviour of Co coated ferritic steel for solid oxide fuel cell interconnects, J. Power Sources. 220 (2012) 217–227. doi:10.1016/j.jpowsour.2012.06.092.

[20] L. Niewolak, D.J. Young, H. Hattendorf, L. Singheiser, W.J. Quadakkers, Mechanisms of Oxide Scale Formation on Ferritic Interconnect Steel in Simulated Low and High pO2 Service Environments of Solid Oxide Fuel Cells, Oxid. Met. 82 (2014) 123–143. doi:10.1007/s11085-014-9481-8.

[21] H. Falk-Windisch, J. Claquesin, M. Sattari, J.-E. Svensson, J. Froitzheim, Co- and Ce/Co-coated ferritic stainless steel as interconnect material for Intermediate Temperature Solid Oxide Fuel Cells, J. Power Sources. 343 (2017) 1–10. doi:10.1016/j.jpowsour.2017.01.045.

[22] P.Y. Hou, J. Stringer, The effect of aluminum as an alloying addition or as an implant on the high-temperature oxidation of Ni-25Cr, Oxid. Met. 34 (1990) 299–321. doi:10.1007/BF00665020.

[23] A. Naoumidis, H.A. Schulze, W. Jungen, P. Lersch, Phase studies in the chromium-manganese-titanium oxide system at different oxygen partial pressures, J. Eur. Ceram. Soc. 7 (1991) 55–63. doi:10.1016/0955-2219(91)90054-4.

[24] A. Petric, H. Ling, Electrical Conductivity and Thermal Expansion of Spinels at Elevated Temperatures, J. Am. Ceram. Soc. 90 (2007) 1515–1520. doi:10.1111/j.1551-2916.2007.01522.x.

[25] A. Holt, P. Kofstad, Electrical conductivity and defect structure of Cr2O3. II. Reduced temperatures (<∼1000°C), Solid State Ionics. 69 (1994) 137–143. doi:10.1016/0167-2738(94)90402-2.

[26] P.Y. Hou, J. Stringer, The effect of reactive element additions on the selective oxidation, growth and adhesion of chromia scales, Mater. Sci. Eng. A. 202 (1995) 1–10. doi:10.1016/0921-5093(95)09798-8.

[27] W.J. Quadakkers, D. Naumenko, E. Wessel, V. Kochubey, L. Singheiser, Growth Rates of Alumina Scales on Fe–Cr–Al Alloys, Oxid. Met. 61 (2004) 17–37. doi:10.1023/B:OXID.0000016274.78642.ae.

[28] J.G. Grolig, J. Froitzheim, J.-E. Svensson, Coated stainless steel 441 as interconnect material for solid oxide fuel cells: Oxidation performance and chromium evaporation, J. Power Sources. 248 (2014) 1007–1013. doi:10.1016/j.jpowsour.2013.08.089.

8 Figure captions

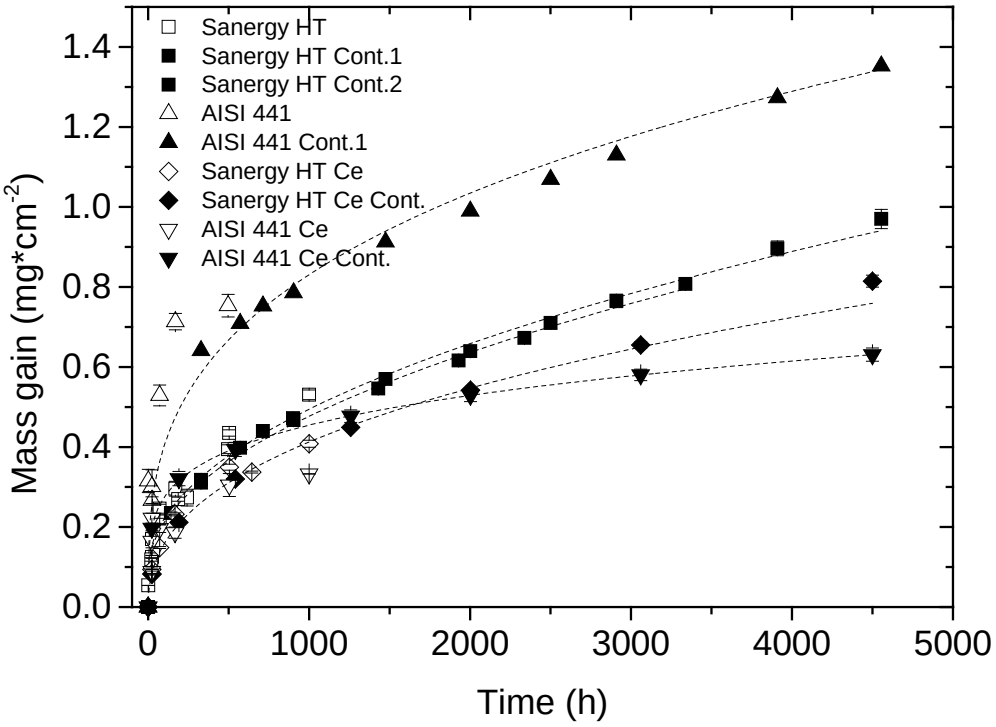

Figure 1. Mass gains plotted against time from all experiments showing both uncoated and Ce-coated samples. Hollow symbols represent data from continuous exposures, and filled symbols represent data from discontinuous exposures. The error bars represent the standard deviation between the samples within the same exposure. The samples were exposed to Ar - 40 % H_2O - 3 % H_2 at 850 °C.

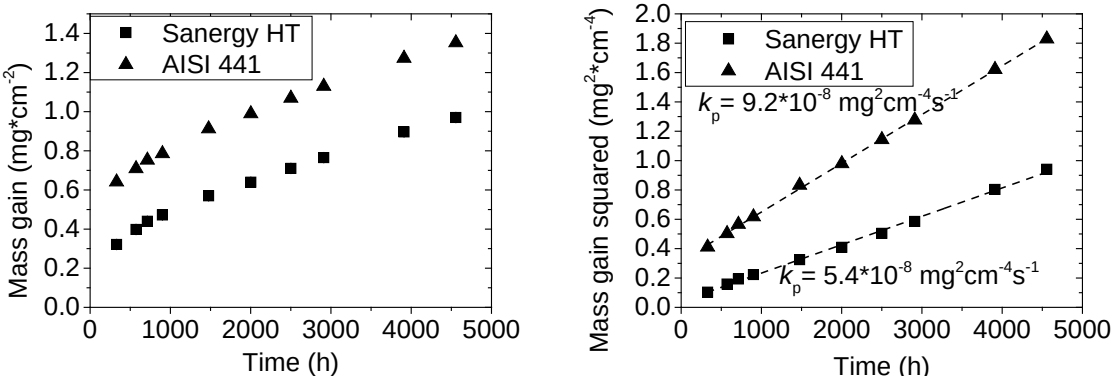

Figure 2. Mass gains (left) and squared mass gains (right) plotted against time for the uncoated steels that were thermally cycled, i.e. the same samples were measured several times. The samples were exposed to Ar - 40 % H_2O - 3 % H_2 at 850 °C.

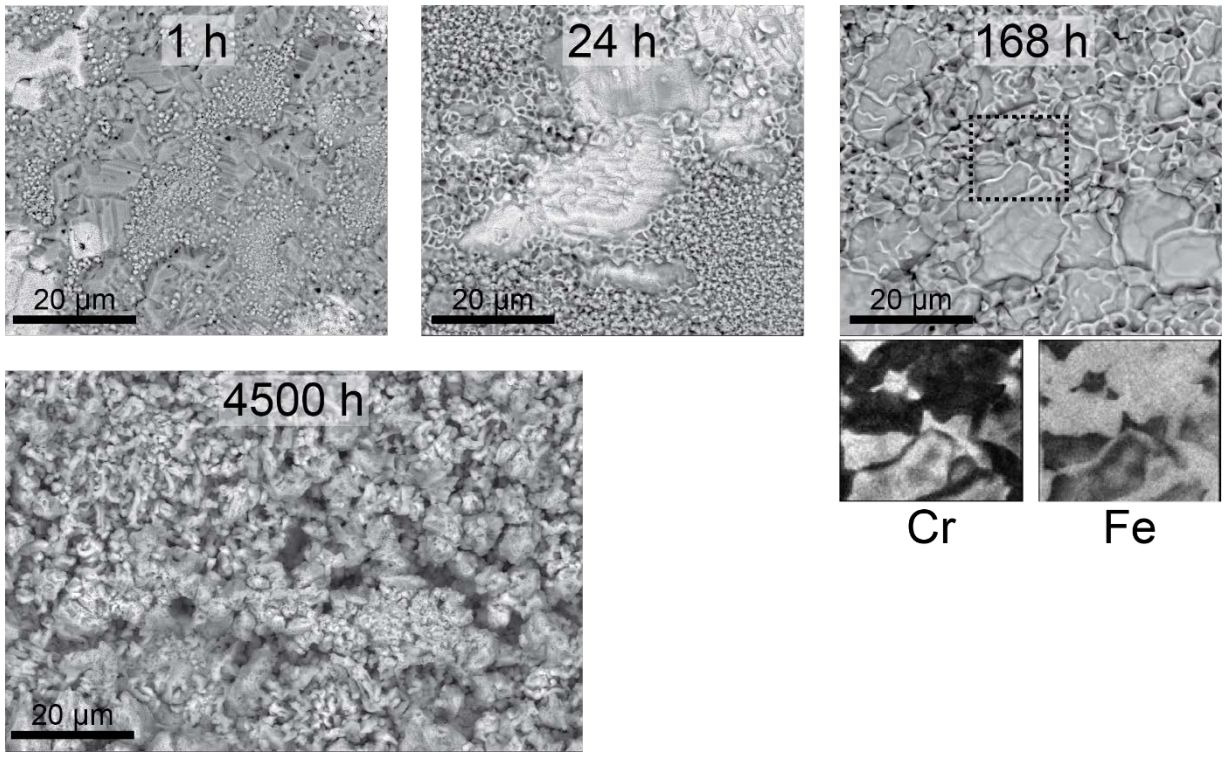

Figure 3. Plan view micrographs and elemental maps of uncoated AISI 441 steel exposed for different periods of time, obtained with SEM/EDX. The samples were exposed to Ar - 40 % H_2O - 3 % H_2 at 850 °C.

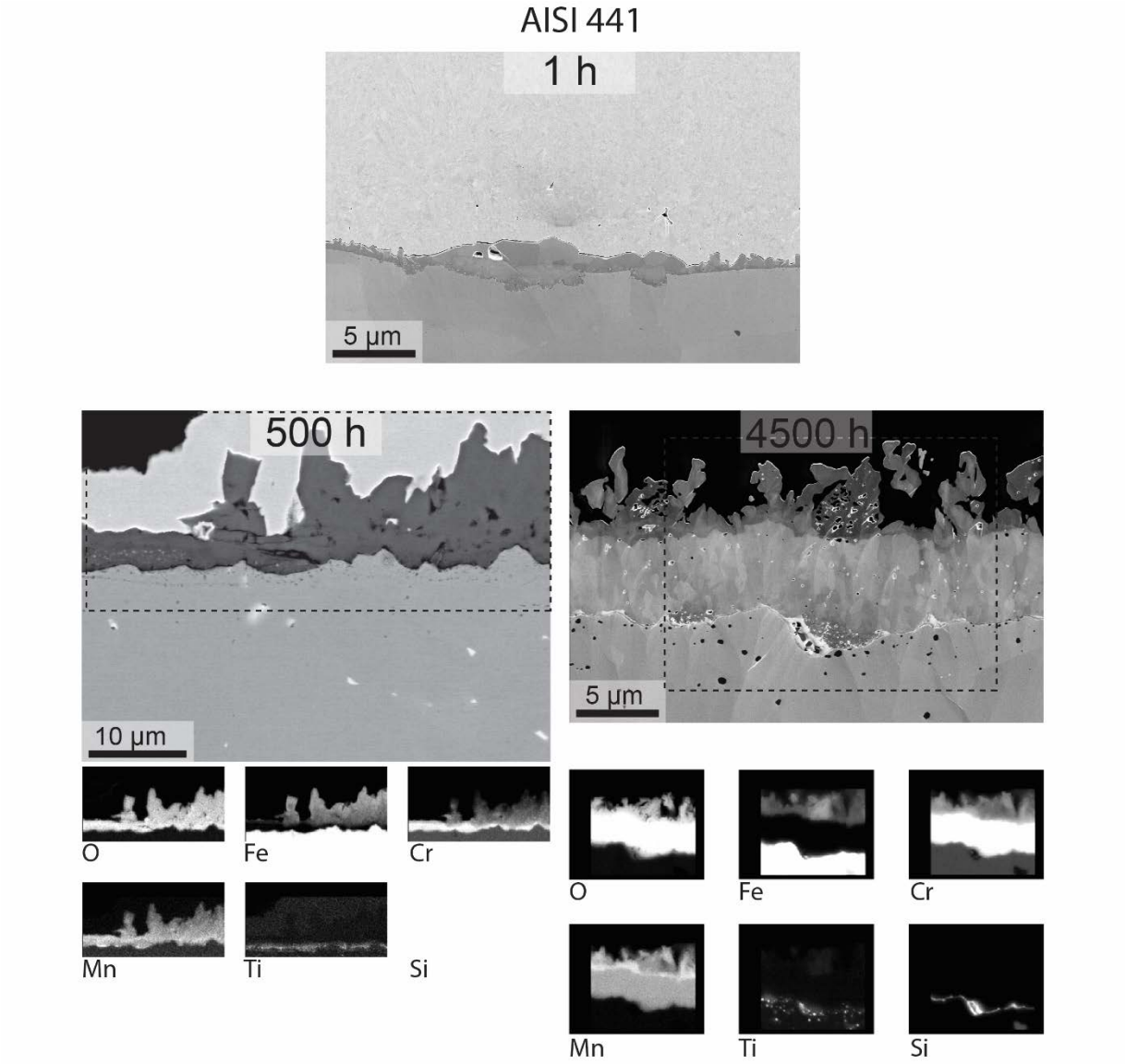

Figure 4. Cross section micrographs and elemental maps of uncoated AISI 441 steel exposed for different periods of time, obtained with SEM/EDX. The samples were exposed to Ar - 40 % H_2O - 3 % H_2 at 850 °C.

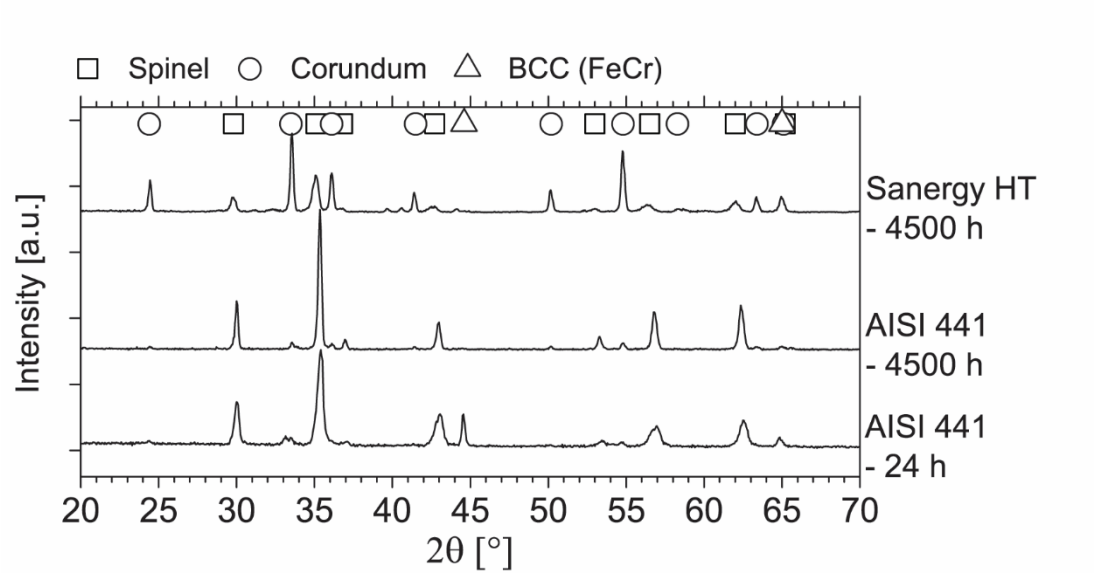

Figure 5. X-ray diffractogram of the uncoated steels after 24-h (AISI 441) and 4500-h exposure to Ar - 40 % H_2O - 3 % H_2 at 850 °C.

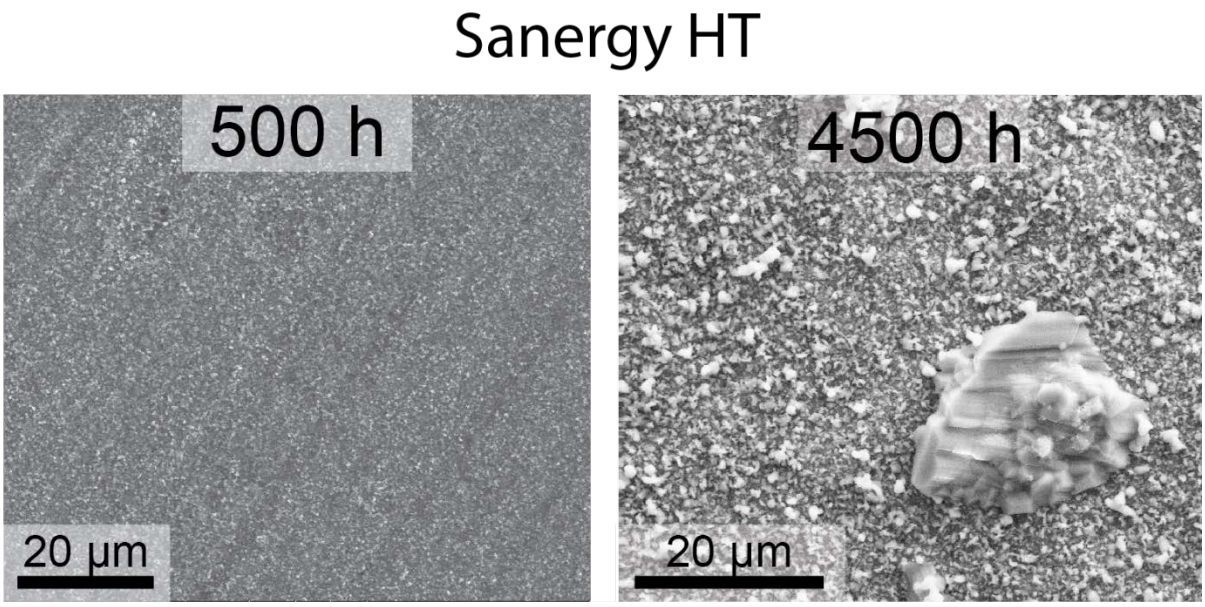

Figure 6. Plan view micrographs and elemental maps of uncoated Sanergy HT exposed for 500 h and 4500 h, obtained with SEM/EDX. The samples were exposed to Ar - 40 % H_2O - 3 % H_2 at 850 °C.

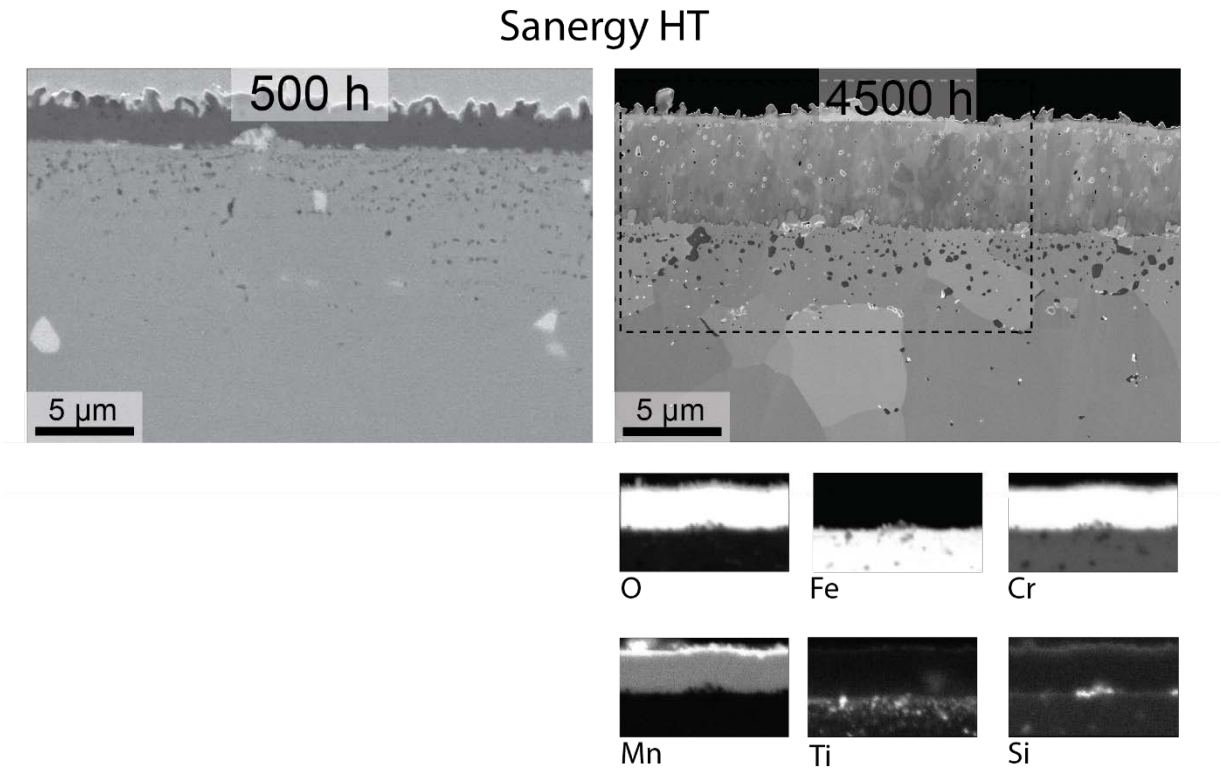

Figure 7. Cross section micrographs and elemental maps of uncoated Sanergy HT exposed for 500 h and 4500 h, obtained with SEM/EDX. The samples were exposed to Ar - 40 % H_2O - 3 % H_2 at 850 °C.

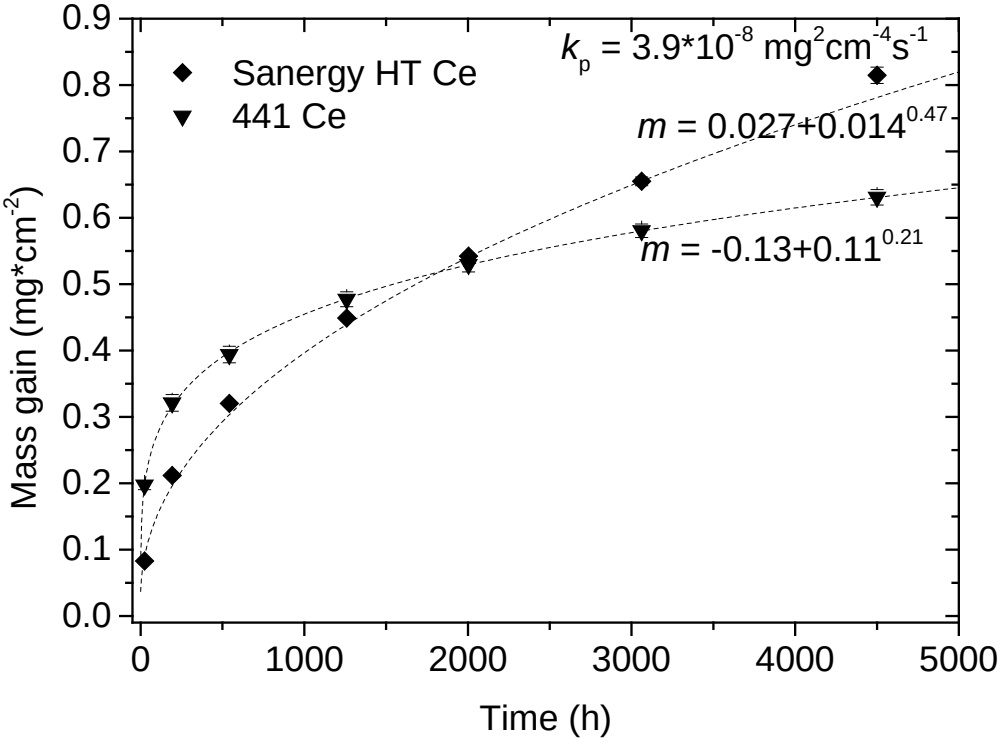

Figure 8. Mass gains plotted against time for the Ce-coated steels that were thermally cycled, i.e. the samples were measured several times. Functions of the form $\Delta m = k_p' * t^X + C'$ have been fitted to the data. The samples were exposed to Ar - 40 % H_2O - 3 % H_2 at 850 °C.

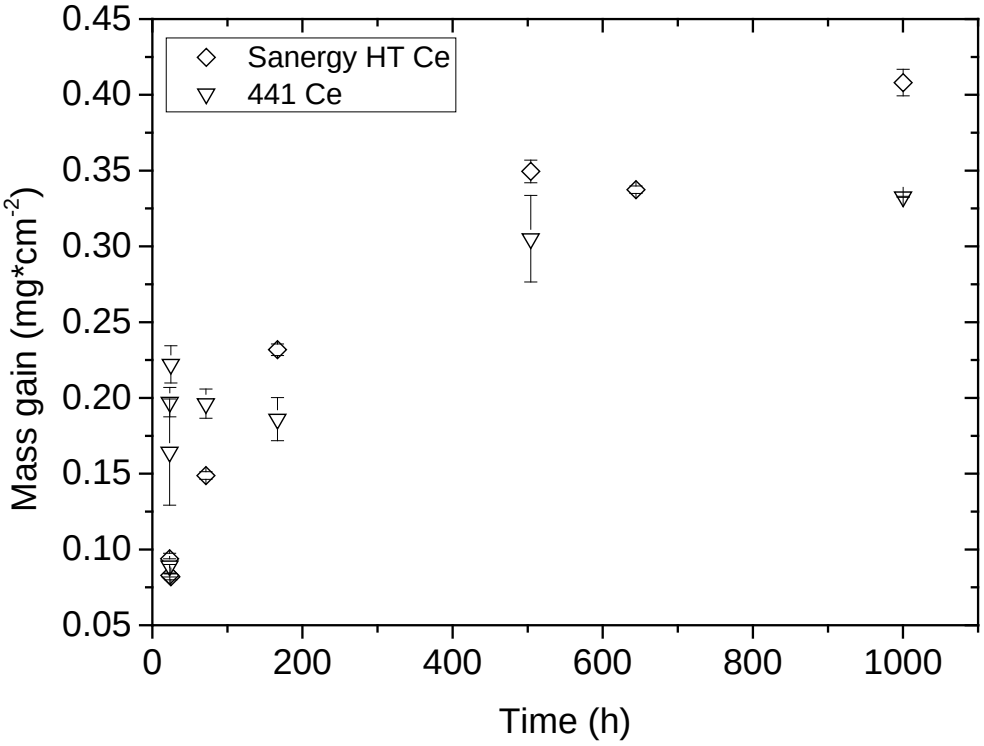

Figure 9. Mass gains plotted against time for the uncoated steels that were exposed once. The letters A and B represent low and high mass gains of AISI 441 steel, respectively, after 24-h exposure, and the corresponding micrographs are presented in Figure 10. The samples were exposed to Ar - 40 % H_2O – 3% H_2 at 850 °C.

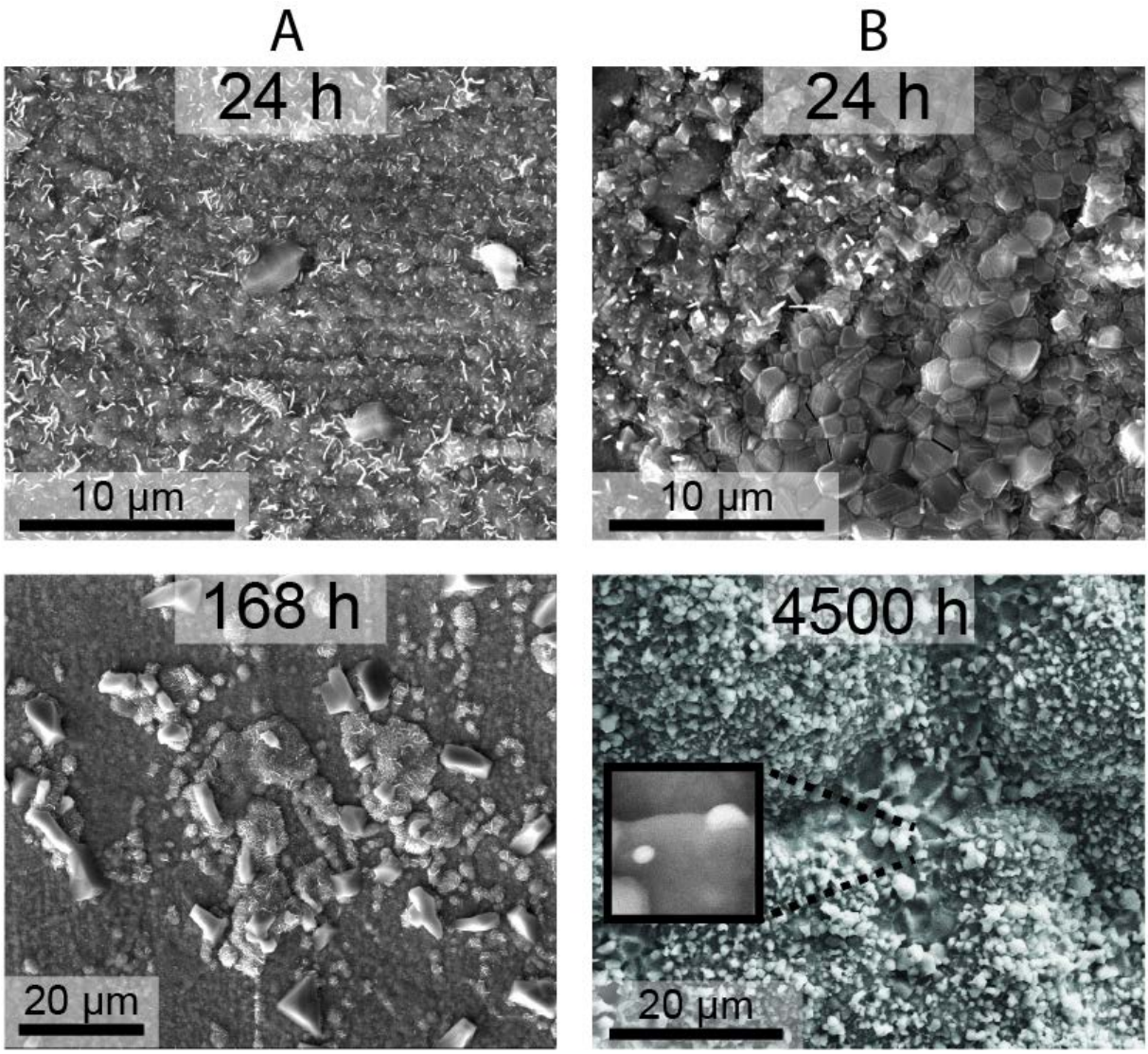

Figure 10. Plan view micrographs of Ce-coated AISI 441 steel exposed for different periods of time, obtained with SEM. The letters A and B represent low and high mass gains of AISI 441steel, respectively, after 24-h exposure, and the corresponding mass gains are presented in Figure 9. The samples were exposed to Ar - 40 % H_2O - 3 % H_2 at 850 °C.

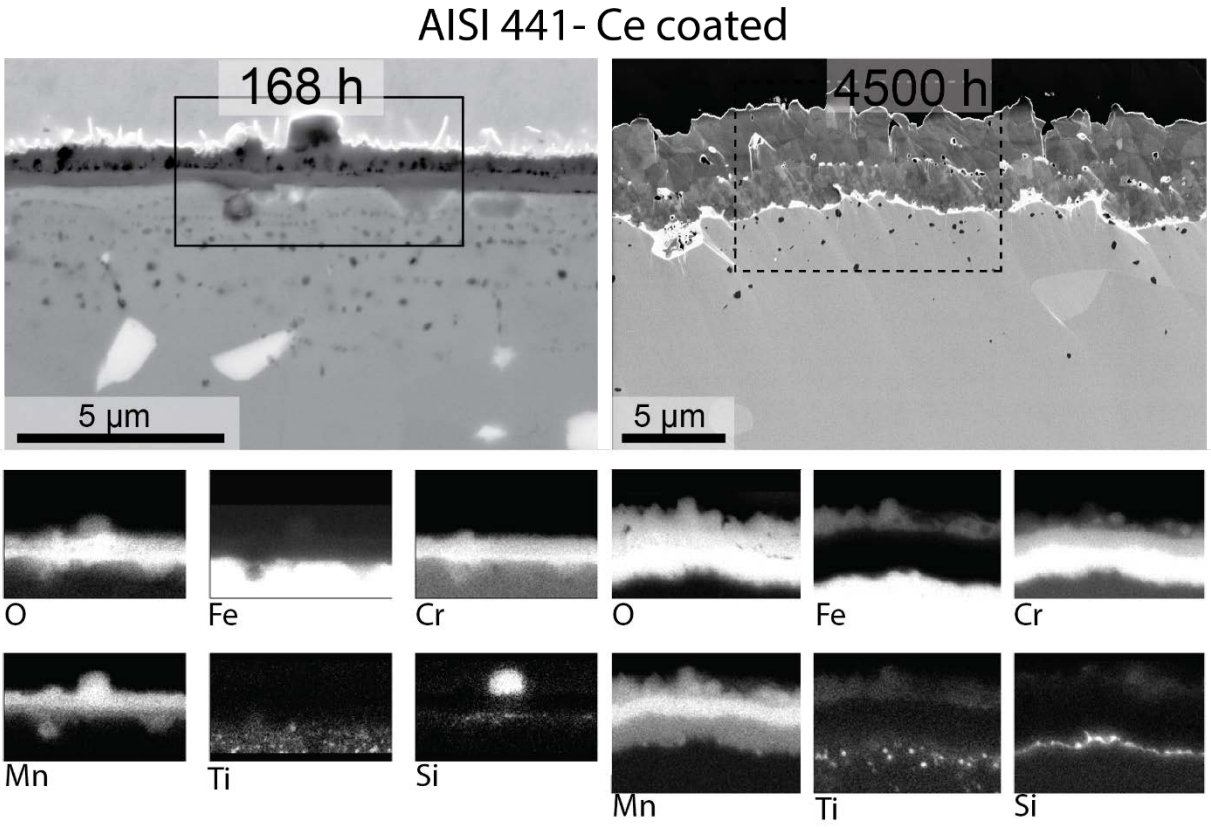

Figure 11. Cross section micrographs and elemental maps of Ce-coated AISI 441 exposed for 168 h and 4500 h, obtained with SEM/EDX. The samples were exposed to Ar - 40 % H_2O - 3 % H_2 at 850 °C.

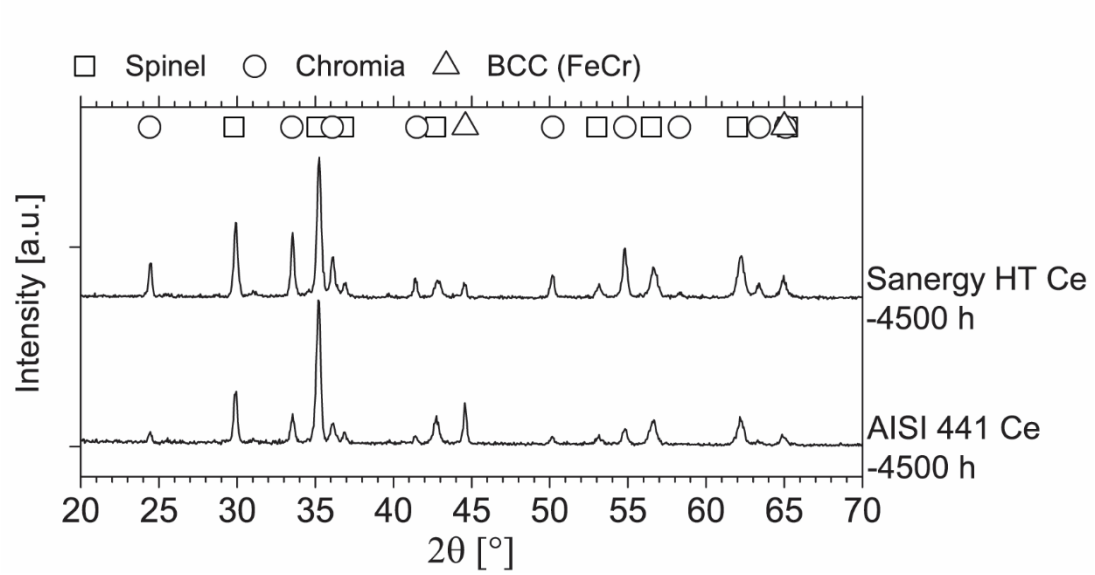

Figure 12. X-ray diffractogram of the uncoated steels after 4500-h exposure to Ar - 40 % H_2O - 3 % H_2 at 850 °C.

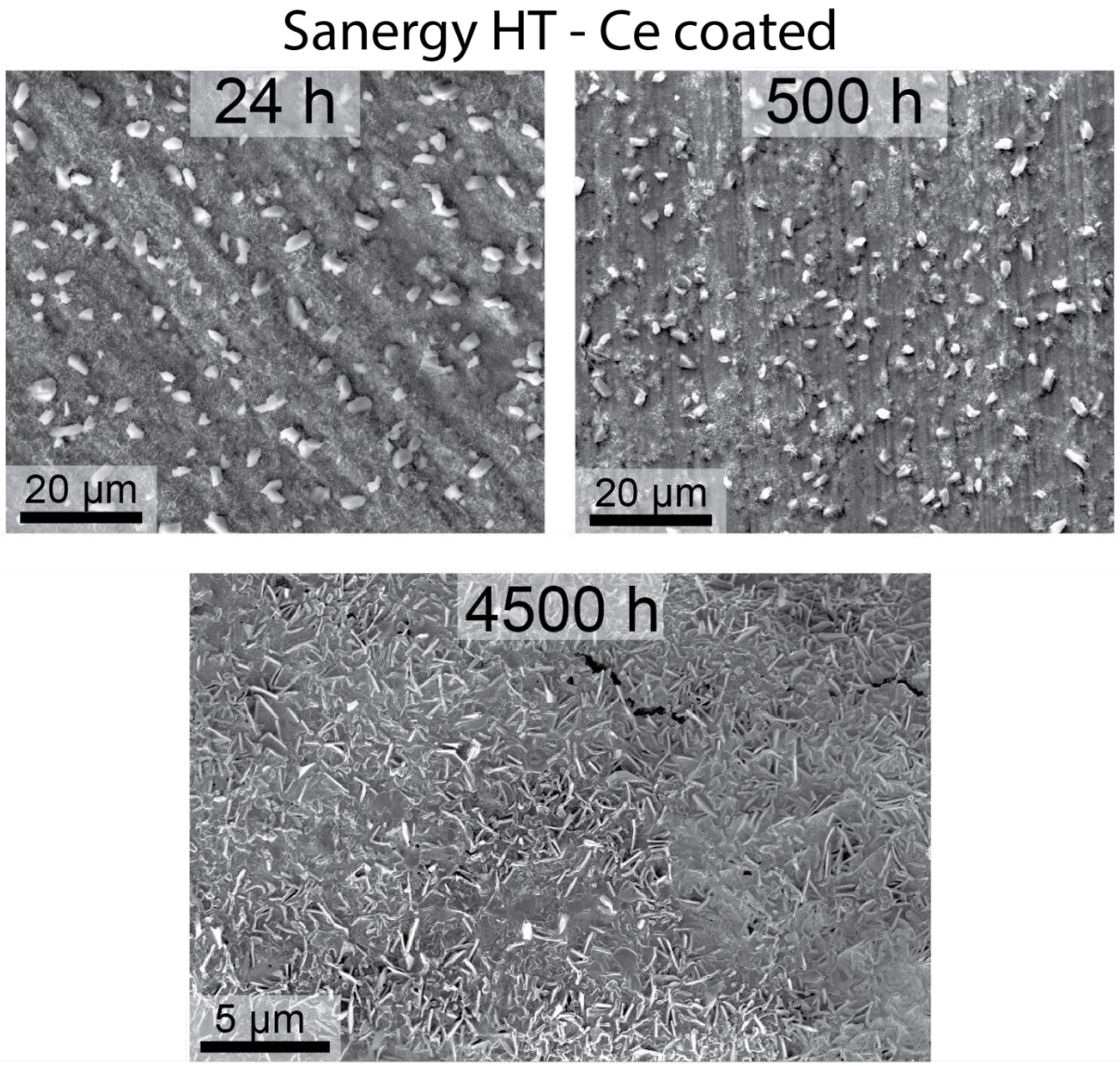

Figure 13. Plan view micrographs and elemental maps of Ce-coated Sanergy HT exposed for 500 h and 4500 h, obtained with SEM/EDX. The samples were exposed to Ar - 40 % H_2O - 3 % H_2 at 850 °C.

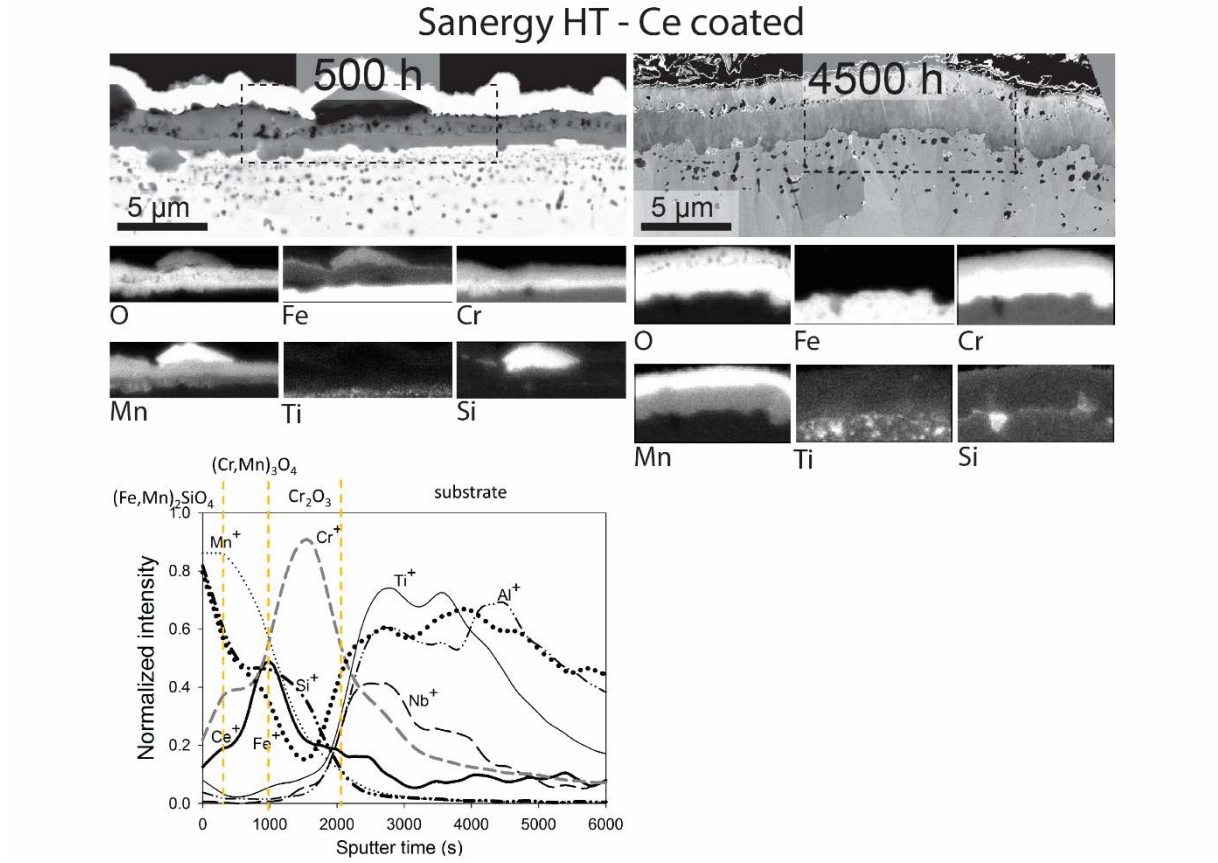

Figure 14. Cross section micrographs and elemental maps of Ce-coated Sanergy HT exposed for 500 h and 4500 h, obtained with SEM/EDX. An element profile for the 500-h sample is also shown, which was obtained with secondary ion mass spectroscopy (SIMS) (Not at the same site as the EDX analysis). The samples were exposed to Ar - 40 % H_2O - 3 % H_2 at 850 °C.

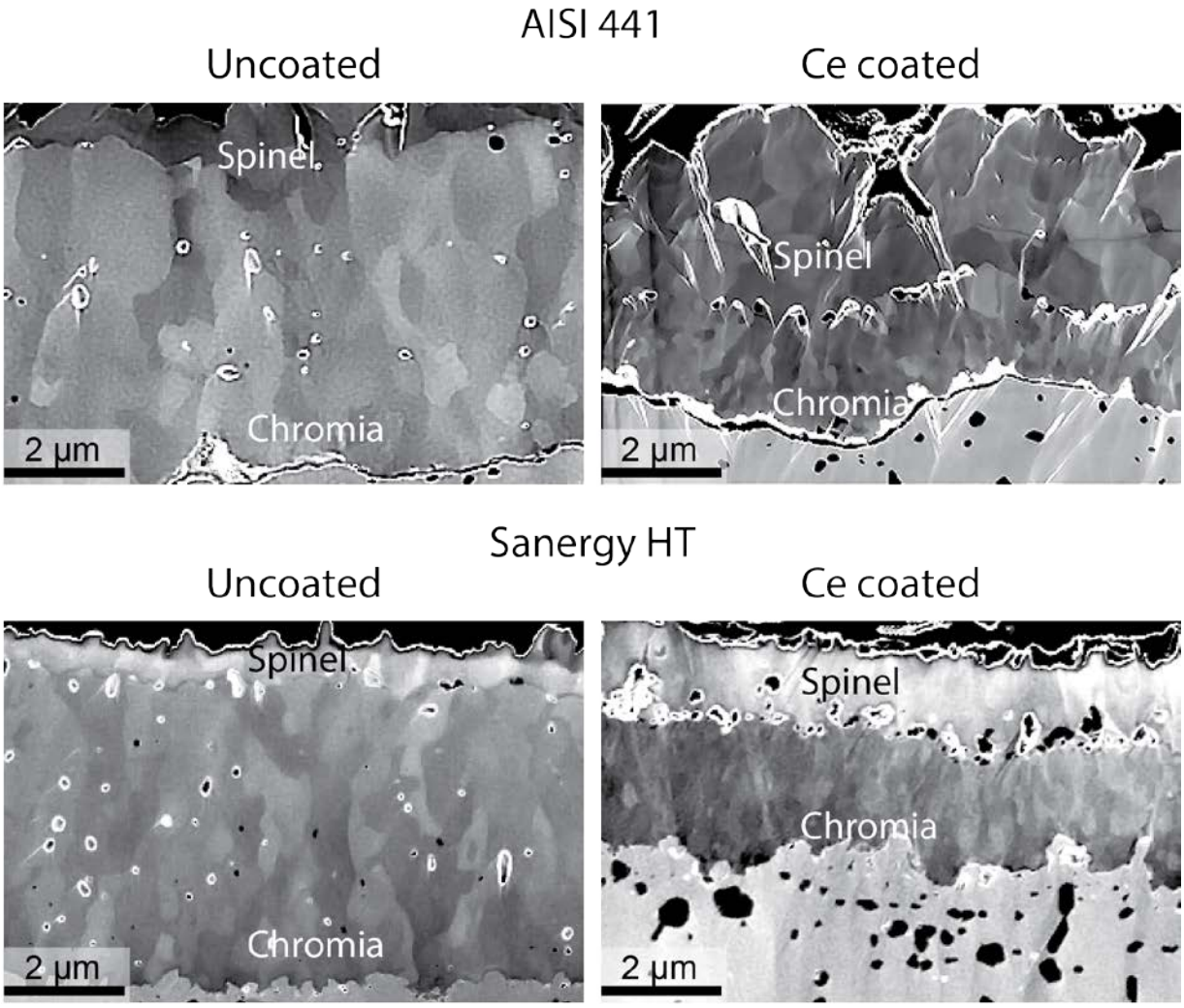

Figure 15. Cross section micrographs of the Cr_2O_3 part of the oxide scales of uncoated and Ce-coated AISI 441 and Sanergy HT steels exposed for 4500 h, obtained with SEM. The samples were exposed to Ar - 40 % H_2O - 3 % H_2 at 850 °C.